THE ASTROPHYSICAL JOURNAL, 474:179–187, 1997 January 1

VLBI OBSERVATIONS OF A COMPLETE SAMPLE OF RADIO GALAXIES. VII. STUDY OF THE FR I SOURCES 3C 31, 4C 35.03, AND 3C 264

L. LARA,[1,2] W. D. COTTON,[3] L. FERETTI,[1,4] G. GIOVANNINI,[1,4] T. VENTURI,[1] AND J. M. MARCAIDE[5]
Received 1996 May 20; accepted 1996 July 19

ABSTRACT

We present results from global VLBI and VLA observations of three Fanaroff-Riley type I radio galaxies, 3C 31, 4C 35.03, and 3C 264, at a frequency of 5 GHz. In all three cases, we observe asymmetric parsec-scale structures consisting of a compact core and a single jet pointing in the direction of the more prominent kiloparsec jet. We interpret such alignment as evidence for the relativistic nature of FR I radio jets at parsec scales. Comparing the VLBI and VLA images of these sources, we find a progressive deceleration of the plasma flow from parsec to kiloparsec scales. We consider another five FR I radio galaxies studied previously by us and find that, in a set of eight FR I objects, the estimated jet bulk velocities and orientation angles with respect to the observer are consistent with the requirements of the unification model for low-power radio sources.

Subject headings: galaxies: individual (3C 31, 4C 35.03, 3C 264) — galaxies: jets — galaxies: structure — radio continuum: galaxies

1. INTRODUCTION

Unified scheme models for radio-loud active galactic nuclei contend that Fanaroff-Riley type I and type II radio galaxies (Fanaroff & Riley 1974) are the misaligned parent populations of BL Lac objects and radio quasars, respectively. During the last few years, a great effort has been made to constrain and test these models by means of detailed studies of individual objects and statistical studies of radio samples (see Antonucci 1993 and Urry & Padovani 1995 for a review). A direct consequence of unification models is that parsec-scale radio jets in FR I and FR II sources should be relativistic, in the same way as they are relativistic in BL Lac objects and quasars. It should then be possible to observe motion of features associated with compressive shocks traveling along the jets. Moreover, orientation-independent differences between BL Lac objects and radio quasars at parsec scales should also be found between FR I and FR II radio sources at the same scales. For example, Lorentz factors seem to be systematically lower in BL Lac objects than in quasars (Mutel 1990), core fractional polarization is usually higher in BL Lac objects, and jet components have magnetic fields oriented preferably perpendicular to the jet axis in BL Lac objects and predominantly parallel in radio quasars (Gabuzda et al. 1994). These and other implications of the unification schemes must be verified through detailed observations of the radio emission from parsec scales in FR I and FR II radio galaxies.

With the primary aims of understanding the nuclear properties of radio galaxies and testing the unification scheme models, we started a program of observations with Very Long Baseline Interferometry (VLBI) of a sample of 27 radio galaxies selected from the B2 and 3CR galaxy samples, having an arcsecond core flux density >100 mJy at 5 GHz (Giovannini, Feretti, & Comoretto 1990). The sample comprises FR I, FR II, and compact sources. We are studying their parsec-scale properties and comparing them with those of more powerful radio sources. Such a study will allow us to derive conclusions about the FR I and FR II populations. Observation and analysis of sources in the sample is near completion; this paper is the seventh of a series dedicated to defining the sample (Giovannini et al. 1990) and to describing in detail the parsec-scale properties of the individual sources (Venturi et al. 1993; Feretti et al. 1993; Giovannini et al. 1994; Cotton et al. 1995; Venturi et al. 1995).

In this paper we present the results derived from new VLBI and Very Large Array (VLA)[6] observations of the FR I radio sources 3C 31, 4C 35.03, and 3C 264. This work adds to that on another five FR I radio sources from our sample: 3C 338, NGC 315, NGC 2484, 0836+29, and 3C 465. We discuss the results from this set of eight FR I radio galaxies, for which good quality VLBI and VLA images are available. As in our previous papers, we assume a Hubble constant $H_0 = 100$ km s^{-1} Mpc^{-1} and a deceleration parameter $q_0 = 1$, and we define the spectral index, α, such that $S_\nu \propto \nu^{-\alpha}$.

2. OBSERVATIONS AND DATA REDUCTION

We observed 4C 35.03 on 1992 June 3 and 3C 31 together with 3C 264 on 1993 February 25, during two VLBI experiments coordinated by the American and European VLBI networks. The observations were made at a frequency of 5 GHz in left circular polarization (LCP) and were scheduled as a series of snapshots, each approximately of half an hour duration. Bright compact radio sources were also observed as fringe finders for the correlation of the VLBI data and as point source calibrators. The antennas participating in each experiment are shown in Table 1, together with the total observing time on each source and the *u-v* range obtained

[1] Istituto di Radioastronomia, CNR, Via Gobetti 101, I-40129 Bologna, Italy.
[2] Instituto de Astrofísica de Andalucía, CSIC, Apdo. 3004, 18080 Granada, Spain.
[3] National Radio Astronomy Observatory, 520 Edgemont Road, Charlottesville, VA 22903-2475.
[4] Dipartimento di Astronomia, Universitá di Bologna, via Zamboni 33, I-40100 Bologna, Italy.
[5] Departamento de Astronomía, Universitat de València, 46100 Burjassot, Valencia, Spain.

[6] The VLA is a facility of the National Radio Astronomy Observatory, which is operated by Associated Universities, Inc., under cooperative agreement with the National Science Foundation.

TABLE 1

OBSERVATIONS

Source	Frequency (MHz)	Array[a]	u-v Range (Mλ)	Observation Time (hr)	Epoch
4C 35.03.....	4973	J, L, S, W, Y, Br, Pt, Nl	0.8–140	9	1992.42
3C 31	4975	E, J, L, W, Y, Br, Hn, La, Nl, Pt, Sc	0.5–141	11	1993.15
3C 264.....	4975	E, J, L, W, Y, Br, Pt, Nl, Hn, La, Sc	2–141	12	1993.15

[a] J: 26 m, Jodrell Bank (England); E: 100 m, Effelsberg (Germany); L: 32 m, Medicina (Italy); S: 25 m, Onsala (Sweden); W: phased array, Westerbork Synthesis Radio Telescope (The Netherlands); Y: phased array, VLA (USA); Br, Pt, Nl, Hn, La, Sc: 25 m each, VLBA-Brewster, Pietown, North Liberty, Hancock, Los Alamos, and Saint Croix respectively (USA).

with the interferometric array. The European stations and the VLA used the Mark-III recording system (Rogers et al. 1983) with a synthesized bandwidth of 28 MHz; the VLBA antennas used a VLBA terminal, recording in a Mark III–compatible mode.

The data from the different telescopes were correlated at the Max-Planck-Institut für Radioastronomie in Bonn (Germany). The calibration of the visibility amplitudes, using the system temperatures and the gain curves from each antenna, and the correction of the fringe rate through the so-called global fringe fitting (Schwab & Cotton 1983), were performed with the NRAO Astronomical Image Processing System (AIPS). The final images were obtained after several cycles of phase and gain self-calibration. We used the AIPS and the Caltech Difmap packages (Shepherd, Pearson, & Taylor 1994), finding in all cases very consistent results in the final images.

VLA data were also recorded, simultaneously to the VLBI data, at the VLA site, allowing us to obtain images of the sources at arcsecond resolution. We calibrated the VLA data with the NRAO AIPS package, using standard VLA calibrators, and after several cycles of self-calibration we obtained images in total intensity and polarization for 4C 35.03 and 3C 264, and only in total intensity for 3C 31.

3. DESCRIPTION OF THE SOURCES

3.1. 3C 31

3C 31 (B2 0104+32) is a low-luminosity radio galaxy identified with NGC 383 [$m_v = 12.14$; $z = 0.0169$; log $P_{\rm tot}(408) = 24.50$ W Hz^{-1}], the brightest member of the chain of galaxies Arp 331 (Arp 1966), and part of the Zwicky cluster 0107.5+3212. The envelope of this galaxy harbors an elliptical companion (NGC 382) located 33″ to the southwest. Owen, O'Dea, & Keel (1990) found an extended emission-line region consistent with a rotating dust ring of radius ~3.″7 reported previously by Butcher, Van Breugel, & Miley (1980). This ring has an inclination of ~40° with respect to the plane of the sky and is probably with its southwest side pointing toward the observer (Fraix-Burnet, Golombek, & Macchetto 1991). X-ray observations with the *Einstein Observatory* reveal extended emission, together with an unresolved component coincident with the radio core (Morganti et al. 1988). High-resolution X-ray data from the ROSAT satellite are also available, but the exposure (2765 s) is too short to allow a reliable determination of the flux density from the nucleus of 3C 31.

3C 31 has been studied previously at radio wavelengths with arcsecond resolutions (e.g., Fomalont et al. 1980; Strom et al. 1983; Andernach et al. 1992). In Figure 1 we show the 5 GHz VLA map obtained from our observations, with an angular resolution of 1.″1. We find an unresolved core with a flux density of 92 mJy, from which two jets depart in position angle (P.A.) of −20°, the northern jet being stronger than the southern one (counterjet). The jet and counterjet bend eastward within ~1.′5 of the core and westward at larger distances. These deflections were interpreted by Blandford & Icke (1978) as the result of a gravitational interaction between NGC 383 and its neighbor NGC 382, but from the analysis of the isophotes of NGC 383 Fraix-Burnet et al. (1991) conclude that there is not, apparently, gravitational interaction between these two galaxies. The surface brightness decreases along the jet and counterjet until the radio structure is resolved completely. In fact, we measure a total length of ~4.′5, much smaller than the ~40′ (~570 kpc) measured by Andernach et al. (1992) from

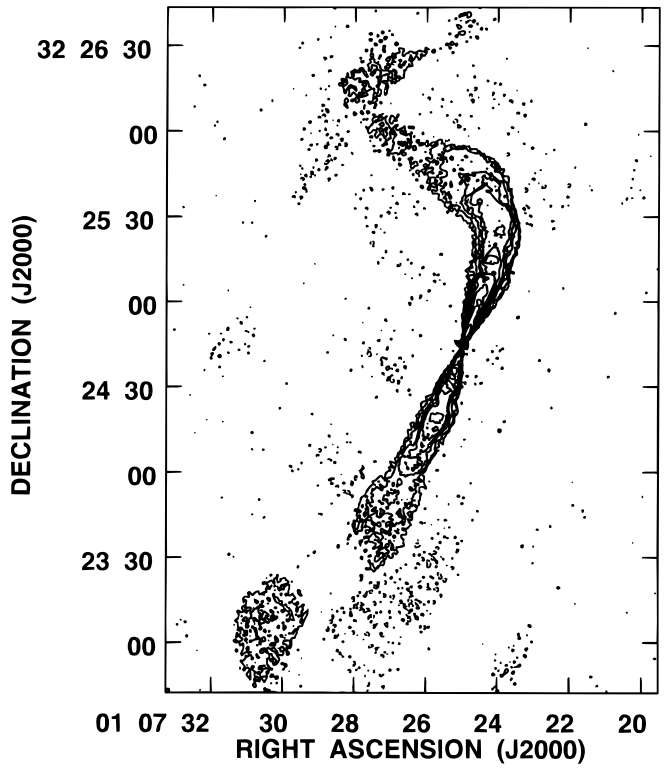

FIG. 1.—VLA image of 3C 31 at 5 GHz. The restoring beam is a circular Gaussian of 1.″1. The peak flux density is 92 mJy beam^{-1}, and the contours are 7.5×10^{-5} Jy beam^{-1} × (−1, 1, 2, 4, 6, 8, 12, 16, 24, 32, 64, 128, 256, 512, 1024, 2048). The rms noise level is 0.02 mJy beam^{-1}.

single-dish observations. Flux density variability in the core of 3C 31 has not been reported in the literature, even if a small level of variability cannot be ruled out (Andernach et al. 1992).

In Figure 2 we display the VLBI map of 3C 31. The image is restored with an elliptical Gaussian beam of 2 mas × 0.9 mas in P.A. = −4°. We presume that the southern component, unresolved and strongest, is the core of the radio source, although such a statement should be confirmed through spectral index determinations. Assuming this core identification, we find a jet extending in P.A. ∼ −15°, slightly different from the P.A. of the stronger jet seen with the VLA (−20°). In order to obtain quantitative estimates of the flux density, positions, and sizes of the VLBI components of 3C 31, we have fitted simple elliptical Gaussian models to the visibility data using a least-squares algorithm. A three-component model provides the best fit to the data (see Table 2), with one component standing for the core and two elongated ones describing the jet structure. The derived total flux density of 3C 31 at VLBI scales is 90 mJy, of which ∼80% comes from the compact core. At a redshift of 0.0169, 1 mas corresponds to a linear distance of 0.24 pc.

3.2. *4C 35.03*

The low-luminosity radio galaxy 4C 35.03 (B2 0206+35) is identified with UGC 1651 [$m_v = 14.3$; $z = 0.0373$; log $P_{tot}(408) = 24.85$ W Hz^{-1}], a galaxy that belongs to the Zwicky cluster 0216.0+3625. The analysis of the isophotes of this galaxy shows evidence of interaction with a nearby companion located at a projected distance of 43″ in P.A. = 110° (González-Serrano & Pérez-Fournon 1991). There is also evidence of a dust lane across the core of UGC 1651 (González-Serrano, Carballo, & Pérez-Fournon 1993). X-ray observations with the *ROSAT* satellite show an unresolved component, possibly dominated by nonthermal emission associated with the inner radio jet, embedded in a resolved thermal component (Worrall & Birkinshaw 1994).

In Figure 3 we display the 5 GHz total intensity VLA map of 4C 35.03, with the linear polarization indicated by line segments whose lengths are proportional to the intensities and whose angles equal the electric vector orientations. The image is restored with an elliptical beam of 8″ × 4″, in P.A. = −84°. With a resolution of 3″.5, the flux density of the core component at 5 GHz is 106 mJy (Morganti et al. 1987). No core flux density variability has been reported in the literature. We find a double symmetric jet extending along the northwest-southeast direction (P.A. = −54°), embedded in a low-brightness halo. The jet directed in the northwest direction appears slightly stronger than the southeast one in the proximities of the central core,

TABLE 2

3C 31: GAUSSIAN FIT PARAMETERS[a]

Component	S (mJy)	D (mas)	P.A. (deg)	L (mas)	r	ϕ (deg)
1	72	...	...	0.7	0.2	−14
2	9	1.5	−16	1.6	<0.1	−16
3	9	6.9	−13	5.1	0.25	−15

[a] For each component we display the flux density (S), the angular distance from the core (D), the position angle (P.A.), the length of the Gaussian major axis (L), the ratio between the major and minor axes (r), and the orientation of the major axis (ϕ) defined in the same sense as the position angle.

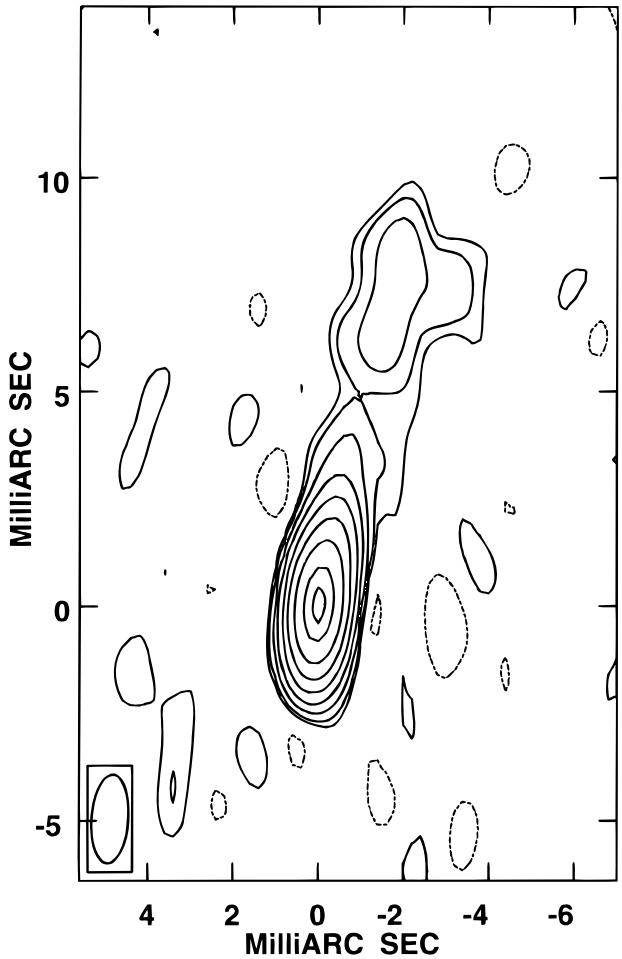

FIG. 2.—VLBI image of 3C 31 at 5 GHz. The restoring beam is an elliptical Gaussian of 2.06 mas × 0.86 mas in P.A. = −4°.1. The peak flux density is 69 mJy beam^{-1}, and the contours are −0.5, 0.5, 1, 2, 4, 6, 8, 16, 32, 64, and 90% of the peak. The rms noise level is 0.20 mJy beam^{-1}.

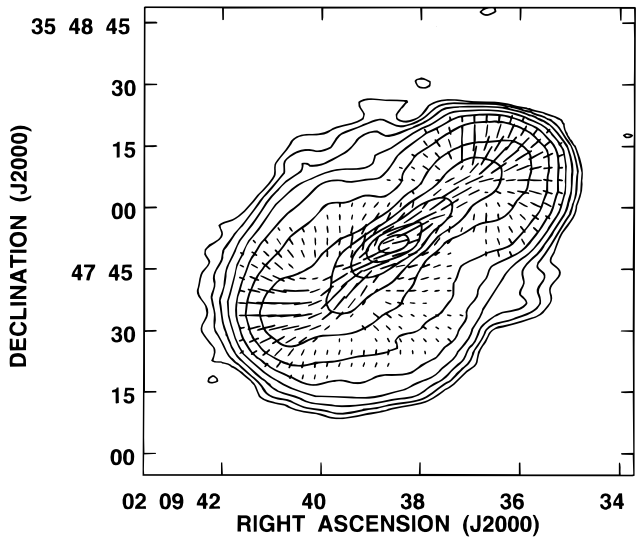

FIG. 3.—VLA image of 4C 35.03 at 5 GHz, with superimposed vectors representing the polarization position angle (E-vector) and length proportional to the amount of polarization. One arcsecond length corresponds to 0.67 mJy beam^{-1}. The restoring beam is an elliptical Gaussian of 8″.02 × 4″.10 in P.A. −84°.5. The peak flux density is 154 mJy beam^{-1}, and the contours are 1 × 10^{-4} Jy beam^{-1} × (−1, 1, 2, 4, 8, 16, 32, 64, 128, 256, 512, 1024). The rms noise level is 0.03 mJy beam^{-1}.

the jet-counterjet brightness ratio being approximately unity at further distances. The brightness distribution has well defined edges in the northwest-southeast direction. We measure a total angular length of $\sim 100''$ (~ 50 kpc), larger than the $67''$ reported by Parma et al. (1987) or the $89''$ reported by Morganti et al. (1987) obtained from previous VLA images with higher angular resolution. The polarization vectors show an ordered magnetic field along the jet and counterjet, essentially perpendicular to the jet axis, obtaining in the lobes a configuration parallel to the outer edges.

We measure the mean fractional polarization (p_m) in the lobes of 4C 35.03 at 5 GHz, obtaining similar values for both: $p_m = 23.2\%$ for the northwest lobe and $p_m = 27.5\%$ for the southeast lobe. Capetti et al. (1993) obtain also a degree of polarization similar for the two lobes, with p_m around 12% at 1.4 GHz. The difference in p_m between the two frequencies could be due to Faraday depolarization produced by material either in front of, or around, 4C 35.03. In the core of 4C 35.03, we measure p_m of 5.6%, while Capetti et al. measure 5.3% at 1.4 GHz. The almost identical values of the core p_m obtained at both frequencies could be understood as due to dominant cellular depolarization related with the observing resolution, which is comparable in the two images. Higher resolution is needed to study the polarization properties of the core of this source. We do not find evidence of the Laing-Garrington effect in 4C 35.03, which could indicate that the source is not favorably oriented toward the observer, and/or that the intrinsic size of the source is too small to show this effect.

In Figure 4 we show the VLBI image of 4C 35.03, restored with a Gaussian beam of 1.5 mas × 1 mas in P.A. = 0°. We find again a one-sided core-jet structure, clearly dominated by the emission from the unresolved component in the southeast extreme, which we identify with the parsec-scale core. The radio structure extends for ~ 5 mas in P.A. = $-50°$, similar to the P.A. of the main jet in the VLA image ($-54°$). No trace of a counterjet is found. Similarly to 3C 31, we have obtained a three-Gaussian elliptical model that reproduces the observed visibilities (see Table 3). The derived total flux density of 4C 35.03 at VLBI scales is 87 mJy, with most of the flux coming from the core component. The linear size conversion factor for this source is 0.51 pc mas^{-1}.

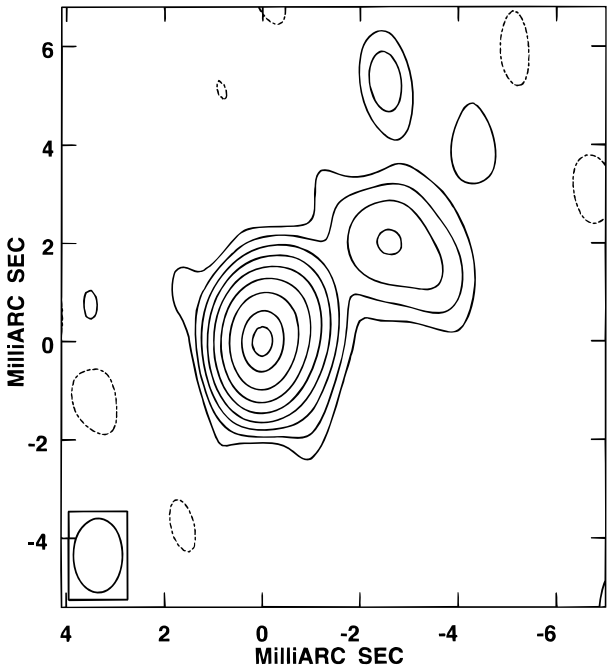

FIG. 4.—VLBI image of 4C 35.03 at 5 GHz. The restoring beam is an elliptical Gaussian of 1.5 mas × 1 mas in P.A. = 0°. The peak flux density is 67 mJy beam^{-1}, and the contours are -0.5, 0.5, 1, 2, 4, 8, 16, 32, 64, and 90% of the peak. The rms noise level is 0.17 mJy beam^{-1}.

3.3. *3C 264*

3C 264 (B2 1142+198) is identified with NGC 3862 [$m_v = 13.67$; $z = 0.0206$; log $P_{\rm tot}(408) = 24.85$ W Hz^{-1}], a bright galaxy in the Abell cluster 1367. A second galaxy can be seen projected on the envelope of NGC 3862, at $\sim 52''$ N from the nucleus. NGC 3862 contains a compact ($\sim 2''$) and possibly variable X-ray source embedded in the diffuse X-ray emission from the intracluster medium in a position consistent with that of the central 5 GHz radio source component (Elvis et al. 1981). Baum et al. (1988) found an oval region of line-emitting gas of $\sim 6''.3$ in extent, centered on the galaxy nucleus, with its major axis oriented almost due east-west, roughly perpendicular to the radio source ejection axis. The optical counterpart of the radio jet, with a length of $\sim 0''.65$ and P.A. $\sim 280°$, was discovered serendipitously with the *Hubble Space Telescope* (Crane et al. 1993), although the synchrotron nature of the feature has yet to be established unambiguously.

In Figure 5 we present the total intensity VLA map of 3C 264. The resolution of the image is $1''.7 \times 1''.6$ with the major axis in P.A. = $-53°$. The radio structure of 3C 264 presents a head-tailed morphology (Gavazzi, Perola, & Jaffe 1981), with a prominent core and a wiggled jet extending toward the northeast. The flux density of the VLA core is ~ 260 mJy. Flux density variability of the core has not been reported in the literature. We find some evidence of a counterjet extending southwest from the core. The jet and counterjet are embedded in a very extended and diffuse emission that fades to the noise level and seems to be dragged along the north. Gavazzi et al. (1981) measure a maximum angular size of $9'$ (~ 160 kpc) (see also Baum et al. 1988; Bridle & Vallé 1981). The main jet emerges from the core with P.A. = 35°, turns to the north at $\sim 4''$ with a large fall in the surface brightness, and turns again to the northeast at about $10''$ from the core. The jet then becomes very weak, almost confused with the diffuse emission, and it ends up in a secondary peak of emission at $35''$ NE of the core. In Figure 6 we show a detailed image of the jet with a resolution of $1''.2 \times 1''.1$ in P.A. = $-62°$, with a linear polarization electric vectors superimposed as in Figure 3. The magnetic field appears parallel to the jet axis in the proximity of the core, becoming perpendicular at an angular distance of $\sim 3''$. The extended emission of 3C 264 has low polarization, and it is difficult to determine the mean fractional polarization of the lobes, since they are not well

TABLE 3

4C 35.03: GAUSSIAN FIT PARAMETERS

Component	S (mJy)	D (mas)	P.A. (deg)	L (mas)	r	ϕ (deg)
1	75	...	...	0.6	0.3	−44
2	4	0.9	−71	1.6	<0.1	−16
3	8	3.4	−49	1.4	0.5	45

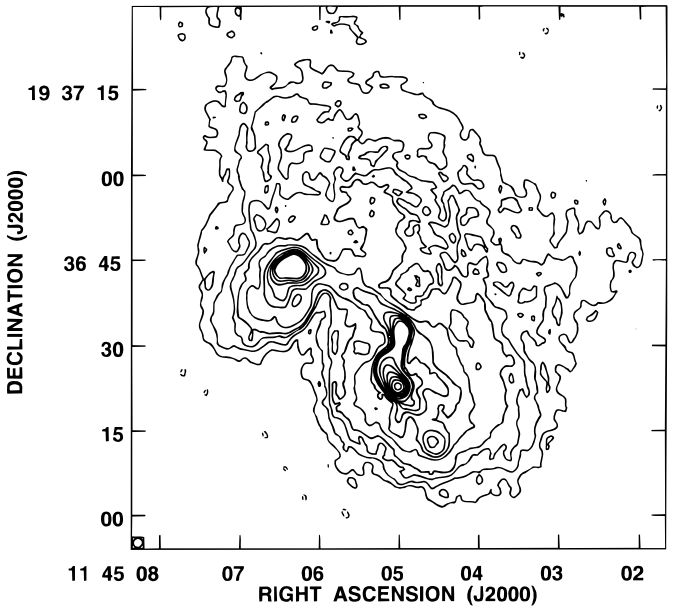

FIG. 5.—VLA image of 3C 264 at 5 GHz. The restoring beam is an elliptical Gaussian of 1.″66 × 1.″61 in P.A. = −53°. The peak flux density is 287 mJy beam^{-1}, and the contours are 2 × 10^{-4} Jy beam^{-1} × (−1, 1, 2, 3, 4, 6, 8, 10, 12, 14, 16, 32, 64, 128, 256, 512, 1024). The rms noise level is 0.06 mJy beam^{-1}.

defined. We obtain a mean fractional polarization of 3.5% in the core and of 5.8% in the northeast region.

The VLBI map of 3C 264 in Figure 7 shows a milliarcsecond-scale structure that consists of a one-sided core-jet extending up to 20 mas from the core and directed in an average P.A. ∼ 27°. There is not any trace of a counterjet. The resolution of the image is 2.9 mas × 0.9 mas with the major axis in P.A. = −7°. We identify the core with the unresolved southernmost component, although a

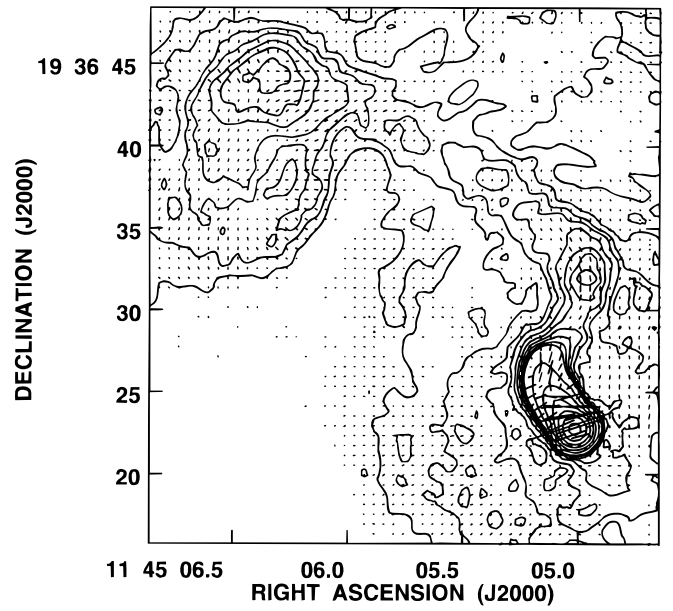

FIG. 6.—Detail of the jet of 3C 264, with polarization vectors superimposed. One arcsecond length corresponds to 1.33 mJy beam^{-1}. The restoring beam is an elliptical Gaussian of 1.″6 × 1.″11 in P.A. = −62°. The peak flux density is 263 mJy beam^{-1} and the contours are 2 × 10^{-4} Jy beam^{-1} × (−1, 1, 2, 3, 4, 6, 8, 10, 12, 14, 16, 32, 64, 128, 256, 512, 1024). The rms noise level is 0.05 mJy beam^{-1}.

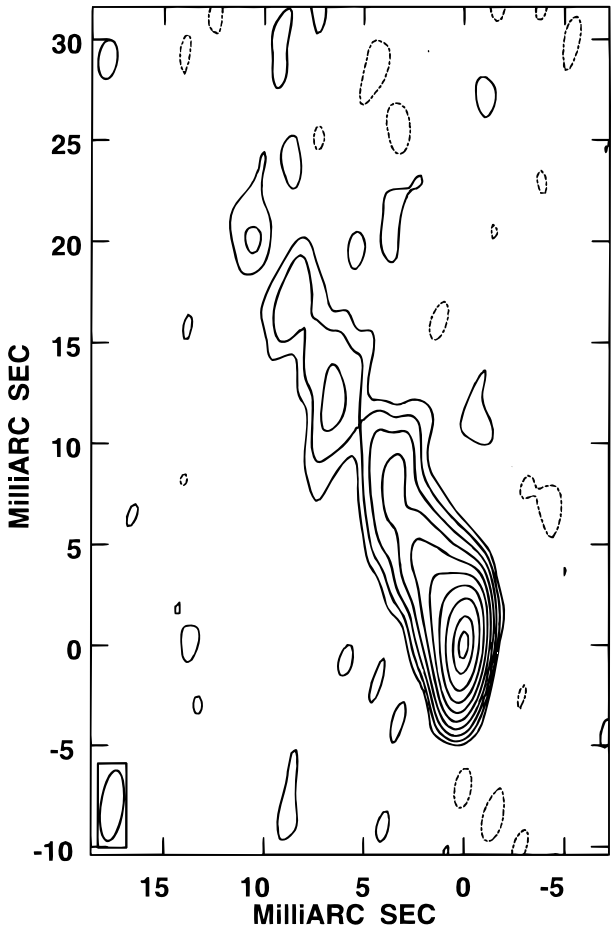

FIG. 7.—VLBI image of 3C 264 at 5 GHz. The restoring beam is 3.5 mas × 1.11 mas in P.A. = −7°.3. The peak flux density is 121 mJy beam^{-1}, and the contours are (−0.25, 0.25, 0.5, 1, 2, 4, 8, 16, 32, 64, and 90% of the peak. The rms noise level is 0.14 mJy beam^{-1}.

spectral index confirmation is needed. Some knots of emission can be distinguished in the map. We have fitted the observed visibilities with a model of three elliptical Gaussian components with parameters displayed in Table 4. The derived total flux density of 3C 264 at VLBI scales is 172 mJy. The linear size conversion factor for this source is 0.29 pc mas^{-1}.

4. LIMITS TO THE JET VELOCITY AND ORIENTATION

The arcsecond-scale structures of 3C 31, 4C 35.03, and 3C 264 show remarkable differences, even though the three sources have similar total radio powers at 408 MHz, i.e., similar unbeamed radio powers. However, at milliarcsecond scales they all show a very similar structure that consists of a compact component and a single jet aligned roughly with the more prominent jet at the arcsecond scale. This asymmetry in the VLBI structure can not be excluded

TABLE 4

3C 264: GAUSSIAN FIT PARAMETERS

Component	S (mJy)	D (mas)	P.A. (deg)	L (mas)	r	ϕ (deg)
1	125	...	...	0.6	0.2	35
2	20	1.7	28	0.9	0.5	41
3	26	4.5	26	8.4	0.1	21

a priori as an intrinsic property of the parsec-scale emission. However, the existence of a parsec-scale jet always on the same side of the main kiloparsec jet reinforces the idea of intrinsically symmetric radio structures seen one-sided at parsec scales due to Doppler-boosted emission from the approaching jet. This adds to the growing evidence on the relativistic nature of the plasma flow in parsec-scale jets of FR I sources (Laing 1993; De Young 1993; Giovannini et al. 1994; Venturi et al. 1995; Maraschi & Rovetti 1994; Parma et al. 1993, 1994; Bicknell 1994).

Under the parsec-scale relativistic-jet scenario for FR I radio sources, we have constrained the possible values of the intrinsic jet velocity (β) and of the orientation of the radio source main axis with respect to the line of sight (θ), following three different approaches: determination of the jet-counterjet brightness ratio, analysis of the correlation between the core and total radio powers, and comparison of the predicted and observed X-ray flux densities in the framework of the synchrotron self-Compton (SSC) model. In 3C 31 an additional constraint can be obtained assuming that its intrinsic linear size is not greater than 1.5 Mpc (see the size-power diagram in De Ruiter et al. 1990). The projected linear size of 3C 31 (0.576 Mpc; Andernach et al. 1992) would then imply an angle to the observer greater than 23°. The allowed regions in the θ-β space deduced from each approach are displayed in Figure 8.

4.1. *Jet-Counterjet Brightness Ratio*

In Table 5 we show the jet-counterjet brightness ratio (R) of 3C 31, 4C 35.03, and 3C 264, measured at different positions along the jet at parsec and kiloparsec scales. In 3C 264, where the definition of the main radio axis is not straightforward, our results refer to the region in which a well-defined and straight jet is observable (the first $\sim 5''$). At parsec scales, where counterjets are not detected, we obtain lower limits of R assuming that the emission from the counterjet is lower than or equal to the rms noise level of the image, measured over large empty regions of the maps. The choice of 1 σ as an upper limit to the counterjet surface brightness is consistent with the other papers of this series and justified given the uniform distribution of residuals in the whole map area, including the assumed counterjet

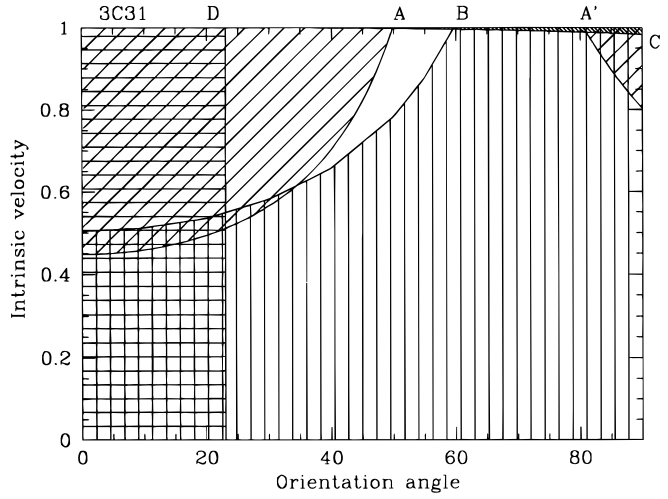

FIG. 8*a*

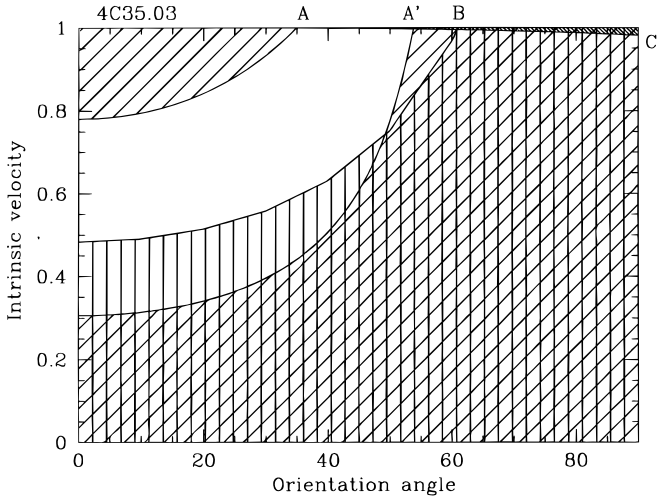

FIG. 8*b*

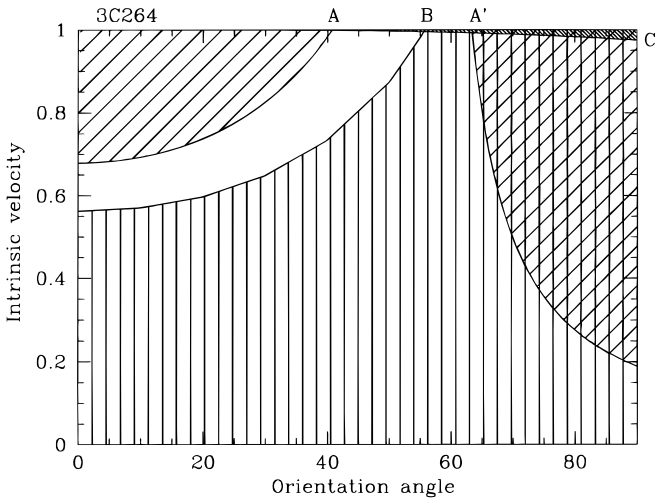

FIG. 8*c*

FIG. 8.—Constraints on the angle θ and the intrinsic jet velocity β for (*a*) 3C 31, (*b*) 4C 35.03, and (*c*) 3C 264. The lines A and A′ correspond to the limits derived from the ratio between the core flux density and the total flux density. Line B is the limit derived from jet/counterjet brightness ratio. Line C corresponds to the lower limit of the Doppler factor derived from X-ray data. Line D in 3C 31 is derived assuming an intrinsic maximum linear size of 1.5 Mpc. In each source, the allowed region is the region without marks.

TABLE 5

JET SIDEDNESS CONSTRAINTS

NAME	VLBI DATA			VLA DATA		
	d (mas)	R	$\beta \cos \theta$	d (arcsec)	R	$\beta \cos \theta$
3C 31	8	>16	>0.504	15	6	0.334
	...	...	...	30	1.5	0.081
4C 35.03	3.5	>14	>0.484	15	1.7	0.106
	...	...	...	30	1.3	0.052
3C 264	5	>24	>0.562	3.3	5	0.311
	10	>18	>0.521	5	2.7	0.196
	15	>4	>0.270	...	...	...

regions. More conservative estimates could be attempted, but we note that the use of 1 σ is still more conservative than other methods found in the literature, such as, for example, the integration of flux density over the counterjet area.

From the relation

$$R = (1 + \beta \cos \theta)^{2+\alpha}(1 - \beta \cos \theta)^{-(2+\alpha)} ,$$

we constrain the possible values of the product $\beta \cos \theta$. This formula assumes intrinsic isotropy of the synchrotron emission, which is a good approximation for our purposes (see the related discussion in Giovannini et al. 1994). We assume a jet spectral index $\alpha = 0.5$.

4.2. *Core Radio Power*

In order to estimate the amount of Doppler boosting independently from the jet sidedness, we make use of a general correlation between the arcsecond core radio power (P_c) and the total radio power (P_t) found by Giovannini et al. (1988) after studying a sample of 187 radio galaxies selected at low frequency:

$$\log P_c = 11.01(\pm 1.05) + 0.47(\pm 0.04) \log P_t .$$

Since the total radio power is measured at low frequency, it is not affected by Doppler boosting. We assume that for a given value of P_t, the dispersion of P_c with respect to the mean regression line reflects different amounts of Doppler boosting produced by different bulk velocities and orientation angles with respect to the line of sight. This assumption is consistent with the results from Parma et al. (1994), who analyzed the B2 radio galaxy sample (included in the sample used to derive the correlation above) and found that the dispersion of the core radio power around the mean regression line can be accounted for by beaming effects, with jet velocities in the range $0.6 < \beta < 0.9$. Hence, assuming that sources are oriented at random angles, the mean regression line would correspond to the mean orientation angle, i.e., 60°. Comparing the estimated value of the core radio power at 60° and the actually measured core radio power, we derive the amount of Doppler boosting and therefore constrain the value of $\beta \cos \theta$ (Giovannini et al. 1994). We use the core flux density measured on the arcsecond scales, since the correlation between the total radio power and the milliarcsecond core radio power is poorly known and still affected by large uncertainties.

We take into account the statistical uncertaintites (1 σ) of the correlation, but the errors in the derived values of $\beta \cos \theta$ are dominated by the possible core flux density variability. Although in the sources discussed here we have not found evidence for significant variability, to be conservative, we allow the core to have a variability up to a factor of 2, thus finding a region of possible values in the β-θ space (between the A and A′ lines in Fig. 8).

4.3. *X-Ray Emission*

We can estimate lower limits to the Doppler factor of a radio source $\{\delta = [\gamma(1 - \beta \cos \theta)]^{-1}$, where the Lorentz factor $\gamma = (1 - \beta^2)^{-1/2}\}$ assuming that the measured X-ray emission from the nuclear region is produced by the SSC process (Marscher 1987; Ghisellini et al. 1993; Urry & Padovani 1995). We assume that the core radio emission is due to synchrotron radiation from a homogeneous sphere, with $\alpha = 0.5$ for the optically thin part of the spectrum. The parameters used in the calculations are given in Table 6: redshift, VLBI core size $D_{\rm VLBI}$, radio flux density S_m at the self-absorption frequency ν_m, and X-ray flux density $S_{\rm X}$ at the energy $h\nu_{\rm X}$. The core size reported in Table 6 for each source is obtained by multiplying the size of the Gaussian fitted for the core component, i.e., the geometric mean of its major and minor axes, by a factor 1.8 in order to obtain a sphere that subtends an equivalent solid angle (Marscher 1987); $D_{\rm VLBI} = 1.8 \times (L^2 r^{-1})^{1/2}$ (L and r are defined as in Tables 2, 3, and 4). Given the lack of VLBI data at other frequencies, we assume that $\nu_m = 5$ GHz. The derived lower limits for the Doppler factor (δ_m) in Table 6 are gross estimates, due to the uncertainties in the self-absorption frequency and the core size and the contamination of the given X-ray flux with contribution of extended thermal emission.

Once a value of δ_m is determined, the allowed region in the β-θ space is delimited by the equation

$$\beta = \frac{\delta_m^2 \cos \theta \pm \sqrt{1 - \delta_m^2 \sin^2 \theta}}{1 + \delta_m^2 \cos^2 \theta} .$$

If $\delta_m > 1$, a lower limit to the velocity and an upper limit to the orientation can be derived from the previous equation: $\beta \geq (\delta_m^2 - 1)/(\delta_m^2 + 1)$; $\theta \leq \arcsin \delta_m^{-1}$ (Ghisellini et al.

TABLE 6

SYNCHROTRON SELF-COMPTON DATA

Name	z	$D_{\rm VLBI}$ (mas)	S_m (mJy)	ν_m (GHz)	$S_{\rm X}$ (μJy)	$h\nu_{\rm X}$ (keV)	δ_m	Reference
3C 31	0.0169	≤0.56	71	5.0	0.038	2.0	≥0.18	1
4C 35.03	0.0373	≤0.59	75	5.0	0.039	1.0	≥0.19	2
3C 264	0.0206	≤0.48	125	5.0	0.790	2.0	≥0.22	3

REFERENCES.—(1) Fabbiano et al. 1984; (2) Worrall & Birkinshaw 1994; (3) Elvis et al. 1981.

1993). But even if $\delta_m < 1$, as in our case, although the previous limits are not valid, constraints to the possible combinations of θ and β can be obtained (see Fig. 8).

5. DISCUSSION

The radio sources presented here, 3C 31, 4C 35.03, and 3C 264, show a very similar asymmetric core-jet parsec-scale structure, which resembles that observed in more powerful radio sources. The parsec-scale jet appears in the same direction of the most prominent kiloparsec-scale jet. As discussed in the previous section, we interpret this radio structure under the parsec-scale relativistic-jet scenario and use available data to constrain the jet velocity and orientation with respect to the line of sight (Fig. 8).

Only for 3C 31 do our data allow the exclusion of the region of very favored orientation with respect to the observer, while for the other two sources no lower limits on the orientation angle could be obtained. The allowed range of θ is $34^\circ \lesssim \theta \lesssim 60^\circ$ for 3C 31, fully consistent with the unified schemes that predict FR I radio galaxies to be at angles $\gtrsim 30^\circ$ (see, e.g., Ghisellini et al. 1993). For this source, the corresponding β range is $0.62 \lesssim \beta \lesssim 0.997$. For 4C 31.04 and 3C 264, the allowed range is $0^\circ \lesssim \theta \lesssim 54^\circ$ and $0^\circ \lesssim \theta \lesssim 55^\circ$, respectively. We note that even if we cannot exclude angles smaller than 30° in these sources, the high jet velocity ($\beta \gtrsim 0.9$) required by the unified schemes is allowed only if $\theta \gtrsim 30^\circ$.

If we assume a roughly constant orientation angle of each jet from parsec to kiloparsec scales, the variation of the jet to counterjet brightness ratio with the distance from the core (Table 5) is consistent with a deceleration of the plasma flow from relativistic velocities at parsec scales to a subrelativistic regime at kiloparsec scales in the jets of our three sources. While the parsec-scale jets have always a relativistic velocity, using the constraints in Table 6 we find for 3C 31 that $\beta \lesssim 0.16$ at deprojected distances larger than 8 kpc from the core; for 4C 35.03, $\beta \lesssim 0.18$ at deprojected distances larger than 10 kpc, and for 3C 264, $\beta \lesssim 0.34$ at deprojected distances larger than 2 kpc. The mechanism of this deceleration is not yet clear. It has been suggested that deceleration in FR I jets could be due to the interaction of radio jets with the interstellar medium (Bicknell 1994; Laing 1996). The fact that the nuclear regions of the galaxies harboring these three radio sources are rich in dust and gas (Owen et al. 1990; González-Serrano et al. 1993; Baum et al. 1988) supports this interpretation.

Taking into account the results obtained on another five FR I radio galaxies studied previously by us, we can compare the allowed range of β-θ values for a total of eight FR I radio galaxies. In Table 7 we show the allowed range for β and the corresponding γ values for all allowed θ values. If unification schemes of FR I radio sources and BL Lac objects are correct, FR I radio sources would have their main radio axis at an angle with respect to the observer exceeding $\sim 30^\circ$ (Ghisellini et al. 1993). Considering this, we also give in Table 7 the γ ranges assuming θ larger than 30° when lower limits in the orientation angle cannot be derived from observational data. Moreover, we assume that the flux density of the core of 3C 338 can be variable in a factor 3, larger than that considered in Giovannini et al. (1994). A more detailed discussion on this source will appear in a future paper (Giovannini et al. 1996b). We note that except for 3C 338, large ($\gtrsim 60^\circ$) orientation angles are not allowed for any of the sources. This result is expected given the core flux density limit introduced in the selection criteria of our sample, and it means that most of our selected radio galaxies have a relatively small angle with respect to the line of sight. Urry & Padovani (1995), comparing the FR I and BL Lac luminosity functions, derive values of γ in the range of 2–20 for radio BL Lac objects, with average values of γ around 3. Our estimates of γ in Table 7 are consistent with this result, supporting the unification schemes of FR I radio sources and BL Lac objects.

Assuming that the derived lower limits in the bulk velocity can also be applied to the velocity of compressive shocks traveling along the jets, they would correspond to apparent velocities that could be detected at VLBI resolutions. However, second epoch observations of FR I radio galaxies show complex and controversial results, suggesting that in FR I jets the apparent velocity could be much lower than the jet velocity (Giovannini et al. 1996a). More observations are planned to investigate this point better.

The parsec-scale radio properties of the studied FR I sources from our sample are very similar, with the exception of 3C 338. They have also similar total radio power at 408 MHz, in the range 10^{24}–10^{25} W Hz^{-1}. However, their kiloparsec-scale structures are quite different. The differences in the kiloparsec-scale morphology and in the linear sizes, in spite of the similar parsec-scale morphology and total radio power at 408 MHz, suggest that the interaction with the external medium plays an important role in the extended structure of these FR I sources. It seems that as

TABLE 7

ORIENTATION-VELOCITY CONSTRAINTS

Name	log P_{tot}(408) (W/Hz)	Orientation (θ)[a] (deg)	Velocity (β)[a]	Gamma (γ)[b]	References
3C 31	24.50	$34 \le \theta \le 60$	$0.62 \le \beta \le 0.998$	$1.27 \le \gamma \le 15.44$	
4C 35.03	24.85	$0 \le \theta \le 54$	$0.48 \le \beta \le 0.999$	$1.14\ (1.21) \le \gamma \le 28.87$	
3C 264	24.85	$0 \le \theta \le 55$	$0.56 \le \beta \le 0.999$	$1.21\ (1.32) \le \gamma \le 18.90$	
NGC 315	23.95	$30 \le \theta \le 41$	$0.78 \le \beta \le 0.969$	$1.60 \le \gamma \le 4.03$	1
NGC 2484.....	25.04	$0 \le \theta \le 46$	$0.55 \le \beta \le 0.999$	$1.20\ (1.40) \le \gamma \le 26.54$	1
3C 338	25.25	$0 \le \theta \le 90$	$0.00 \le \beta \le 0.711$	$1.00 \le \gamma \le 1.42$	1
0836+29	25.08	$0 \le \theta \le 37$	$0.75 \le \beta \le 0.999$	$1.51\ (2.29) \le \gamma \le 24.06$	2
3C 465	25.30	$0 \le \theta \le 53$	$0.60 \le \beta \le 1.0$	$1.25\ (1.35) \le \gamma$	2

[a] Not all the combinations of allowed values of θ and β are possible, as evidenced from Fig. 8.

[b] A lower limit on γ assuming an orientation angle of 30° is displayed in parentheses for those sources for which lower limits on the orientation angle cannot be derived from the observational data.

REFERENCES.—(1) Giovannini et al. 1994; (2) Venturi et al. 1995).

soon as the jet decelerates to a subrelativistic velocity, the external medium affects strongly the source properties to produce the very different kiloparsec-scale morphologies, independently from the parsec-scale properties. In 4C 35.03, the smaller linear size and the configuration of the magnetic field at the edges of the radio structure could indicate the existence of a particularly high density medium confining the radio emission. It is important to note that FR I radio galaxies are usually found in dense environments rich of galaxies (Hill & Lilly 1991). In particular, all sources discussed here belong to clusters or groups of galaxies in which the existence of an intracluster medium is supported by the detection of diffuse thermal X-ray emission.

6. CONCLUSIONS

We present VLBI and VLA images of the radio galaxies 3C 31, 4C 35.03, and 3C 264, which contribute to deciphering the properties of FR I type radio sources at parsec scales. Historically, the study of the parsec-scale emission from FR I sources has been limited to the few cases with higher flux densities (M87, NGC 6251). Hence, it is of great importance to increase the sample of studied FR I radio galaxies at high angular resolution.

In the three sources discussed in this paper, we find similar one-sided core-jet radio structures at parsec resolution, pointing in the direction of the more prominent kiloparsec jet in each source. Such alignment is similarly observed in other FR I radio sources from our sample, supporting the growing evidence that radio jets in low-power FR I radio galaxies are relativistic at parsec scales. In the framework of the relativistic jet model, we constrain the values of the orientation angle of the jet and of the intrinsic velocity of the plasma flow. We obtain allowed values for the γ factor in a range compatible with that obtained by Urry & Padovani (1995) for BL Lac objects. The constraints obtained on the orientation angles are also consistent with the requirements of low power unification schemes.

Based on jet-to-counterjet brightness ratio measurements, we find evidence of a deceleration of the plasma flow from relativistic velocities at parsec scales to subrelativistic at kiloparsec scales. The study of the transition region between these two regimes, probably at sub-arcsecond resolutions, would be crucial to understand the deceleration mechanisms in FR I radio galaxies.

We acknowledge F. Mantovani and D. Dallacasa for critical reading of the manuscript. L. L. acknowledges a postdoctoral fellowship from the Spanish CSIC. We thank the staff at the telescopes and at the correlator in Bonn for their assistance.

REFERENCES

Andernach, H., Ferretti, L., Giovannini, G., Klein, U., Rossetti, E., & Schnaubelt, J. 1992, A&AS, 93, 331
Antonucci, R. 1993, ARA&A, 31, 473
Arp, H. C. 1966, Atlas of Peculiar Galaxies (Pasadena: California Inst. of Technology)
Baum, S. A., Heckman, T., Bridle, A., Van Breugel, W., & Miley, G. 1988, ApJS, 68, 643
Bicknell, G. V. 1994, ApJ, 422, 542
Blandford, R. D., & Icke, V. 1978, MNRAS, 185, 527
Bridle, A. H., & Vallée, J. P. 1981, AJ, 86, 1165
Butcher, H. R., Van Breugel, W., & Miley, G. K. 1980, ApJ, 235, 749
Capetti, A., Morganti, R., Parma, P., & Fanti, R. 1993, A&AS, 99, 407
Cotton, W. D., Feretti, L., Giovannini, G., Venturi, T., Lara, L., Marcaide, J., & Wehrle, A. E. 1995, ApJ, 452, 605
Crane, P., et al. 1993, ApJ, 402, L37
De Ruiter, H., Parma, P., Fanti, C., & Fanti, R. 1990, A&A, 227, 351
De Young, D. S. 1993, ApJ, 405, L13
Elvis, M., Schreier, E. J., Tonry, J., Davis, M., & Huchra, J. P. 1981, ApJ, 246, 20
Fabbiano, G., Miller, L., Trinchieri, G., Longair, M., & Elvis, M. 1984, ApJ, 277, 115
Fanaroff, B. L., & Riley, J. M. 1974, MNRAS, 167, 31
Feretti, L., Giovannini, G., Venturi, T., & Wehrle, A. E. 1993, ApJ, 408, 446
Fomalont, E. B., Bridle, A. H., Willis, A. G., & Perley, R. A. 1980, ApJ, 237, 195
Fraix-Burnet, D., Golombek, D., & Macchetto, F. D. 1991, AJ, 102, 562
Gabuzda, D. C., Mullan, C. M., Cawthorne, T. V., Wardle, J. F. C., & Roberts, D. H. 1994, ApJ, 435, 140
Gavazzi, G., Perola, C. G., & Jaffe, W. 1981, A&A, 103, 35
Ghisellini, G., Padovani, P., Celotti, A., & Maraschi, L. 1993, ApJ, 407, 65
Giovannini, G., Cotton, W. D., Lara, L., & Venturi, T. 1996a, in Extragalactic Radio Sources, ed. R. Eckers, C. Fanti, & L. Padrielli (Dordrecht: Kluwer), in press
Giovannini, G., Feretti, L., & Comoretto, G. 1990, ApJ, 358, 159
Giovannini, G., Feretti, L., Gregorini, L., & Parma, P. 1988, A&A, 199, 73
Giovannini, G., Feretti, L., Venturi, T., Lara, L., Marcaide, J., Rioja, M., Spangler, S. R., & Wehrle, A. E. 1994, ApJ, 435, 116
Giovannini, G., et al. 1996b, in preparation
González-Serrano, J. I., Carballo, R., & Pérez-Fournon, I. 1993, AJ, 105, 1710
González-Serrano, J. I., & Pérez-Fournon, I. 1991, A&A, 249, 75
Hill, G. J., & Lilly, S. J. 1991, ApJ, 367, 1
Laing, R. A. 1993, in Astrophysical Jets, ed. M. Fall et al. (Cambridge: Cambridge Univ. Press), 26
Laing, R. A. 1996, in Extragalactic Radio Sources, ed. R. Eckers, C. Fanti, & L. Padrielli (Dordrecht: Kluwer), in press
Maraschi, L., & Rovetti, F. 1994, ApJ, 436, 79
Marscher, A. P. 1987, in Superluminal Radio Sources, ed. A. Zensus & T. J. Pearson (Cambridge: Cambridge Univ. Press), 280
Morganti, R., Fanti, C., Fanti, R., Parma, P., & Ruiter, H. R. 1987, A&A, 183, 203
Morganti, R., Fanti, R., Gioia, I. M., Harris, D. E., Parma, P., & de Ruiter, H. R. 1988, A&A, 189, 11
Mutel, R. L. 1990, in Parsec-Scale Radio Jets, ed. A. Zensus & T. J. Pearson (Cambridge: Cambridge Univ. Press), 98
Owen, F. N., O'Dea, C. P., & Keel, W. C. 1990, ApJ, 352, 44
Parma, P., de Ruiter, H. R., Fanti, R., & Laing, R. A. 1994, in First Stromlo Symp. on the Physics of Active Galaxies, ed. G. V. Bicknell et al. (San Francisco: ASP), 241
Parma, P., Fanti, C., Fanti, R., Morganti, R., & de Ruiter, H. R. 1987, A&A, 181, 244
Parma, P., Morganti, R., Capetti, A., Fanti, R., & de Ruiter, H. R. 1993, A&A, 267, 31
Rogers, A. E. E., et al. 1983, Science, 219, 51
Schwab, F. R., & Cotton, W. D. 1983, AJ, 88, 688
Shepherd, M. C., Pearson, T. J., & Taylor, G. B. 1994, BAAS, 26, 987
Strom, R. G., Fanti, R., Parma, P., & Ekers, R. D. 1983, A&A, 122, 305
Urry, C. M., & Padovani, P. 1995, PASP, 107, 803
Venturi, T., Castaldini, C., Cotton, W. D., Feretti, L., Giovannini, G., Lara, L., Marcaide, J., & Wehrle, A. E. 1995, ApJ, 454, 735
Venturi, T., Giovannini, G., Feretti, L., Comoretto, G., & Wehrle, A. E. 1993, ApJ, 408, 81
Worrall, D. M., & Birkinshaw, M. 1994, ApJ, 427, 134